doi.org/10.36721/PJPS.2026.39.7.207.1

Effects of curcumin on the signal transducer and activator of transcription 3 signaling pathway and bile acid enterohepatic circulation in liver cancer mice model

Na Hu[1#], Niu Yan[2#], Tingting Zhao[3] and Langui Hu[2]*

[1]Department of Medical Affairs, Shanxi Provincial Hospital of Traditional Chinese Medicine, Taiyuan, Shanxi, 030012, China
[2]Pinghe Branch of Shanxi Provincial Hospital of Traditional Chinese Medicine, Taiyuan, Shanxi, 030012, China
[3]Department of Acupuncture, Shanxi Provincial Hospital of Traditional Chinese Medicine, Taiyuan, Shanxi, 030012, China

Abstract: **Background**: Liver cancer has a high incidence and poor prognosis. Curcumin is a natural compound with anti-tumor activity, but its effects on the STAT3 signaling pathway and the bile acid enterohepatic circulation in liver cancer models remain unclear. **Objectives**: To investigate the effects of curcumin on the STAT3 signaling pathway and bile acid enterohepatic circulation in a mouse model of liver cancer. **Methods**: A liver cancer model was established in C57BL/6J mice, which were divided into a sham surgery group, a model control group, low-, medium- and high-dose curcumin groups, a STAT3 inhibitor group, a combination intervention group and a cisplatin positive control group. HE staining was used to observe the pathological morphology of liver tissue. Serum biochemical indicators and IL-6 and TGF-β1 levels were measured. STAT3 pathway proteins were detected by Western blot and related gene expression was analyzed by qRT-PCR. **Results**: Curcumin dose-dependently inhibited STAT3 signaling activity and reduced the p-STAT3/total STAT3 ratio ($P<0.05$). In the high-dose curcumin group, serum ALT, AST and TB levels decreased from (254.55±56.14)U/L, (542.01±71.28)U/L and (42.98±8.21)μmol/L to (47.98±10.68)U/L, (135.24±24.12)U/L and (7.91±1.36)μmol/L, respectively (all $P<0.05$). Curcumin upregulated the expression of BSEP, NTCP and FXR, downregulated Cyp7a1 and upregulated the expression of intestinal Fgf15 and Asbt. **Conclusion**: Curcumin alleviates liver injury and inflammation while ameliorating bile acid enterohepatic circulation by inhibiting the STAT3 signaling pathway.

Keywords: Curcumin; Enterohepatic circulation; Liver cancer; STAT3

Submitted on 26-11-2025 – Revised on 31-12-2025 – Accepted on 26-01-2026

INTRODUCTION

Bile acid enterohepatic circulation is the recycling process by which bile acids are transported between the liver and the intestines (Zhu *et al*., 2023). On the one hand, it is involved in lipid digestion and cholesterol metabolism, both of which are very important for maintaining normal function. On the other hand, if the enterohepatic circulation of bile acids is disturbed, adverse effects can occur on the liver and intestines. Studies have reported (Fleishman and Kumar, 2024; Xie *et al*., 2021) that the accumulation of bile acids may lead to cholestasis and liver cell damage and that abnormal bile acid metabolism is also associated with obesity, type 2 diabetes and other diseases. At the same time, the occurrence of liver cancer often leads to abnormal enterohepatic circulation of bile acids and there are currently few studies on this aspect. Therefore, it is crucial to find safe and effective drugs and explore their mechanisms. The STAT3 signaling pathway can be inhibited by various natural products, thereby exerting anti-hepatocellular carcinoma effects. Xanthohumol can suppress the STAT3 signaling pathway, reduce the expression of Bcl-2 and cyclin D1 and consequently mediate the inhibition of hepatocellular carcinoma (Girisa *et al*., 2021). Ginsenosides can also inhibit low STAT3 expression, which promotes apoptosis of liver cancer cells (Tan *et al*., 2023). White glycine acid can also inhibit STAT3, reduce TLR4 expression and inhibit phosphorylation of AMPK/LKB1 (Cui *et al*., 2021), thereby reducing the degree of liver fibrosis. Although STAT3 inhibition has shown positive effects in combating hepatocellular carcinoma, it remains unclear whether it improves abnormalities in the enterohepatic circulation of bile acids by regulating this pathway, which warrants further investigation.

Curcumin is a natural compound extracted from the rhizome of the turmeric plant. It possesses various biological activities, such as scavenging free radicals, exerting antioxidant effects and inhibiting inflammatory responses. In terms of anti-tumor activity, curcumin can inhibit the progression of hepatocellular carcinoma by downregulating Cyclin D1 and MMP-2, upregulating E-cadherin, promoting miR-29 expression and inhibiting VEGF (Su *et al*., 2025; Wang *et al*., 2023). Moreover, curcumin can also inhibit the capabilities of HepG2 cells (Ghufran *et al*., 2022; Ma *et al*., 2025) and EMT process of cells through NF-κB/Snail pathway to prevent damage to the enterohepatic circulation of bile acids (Pouliquen *et al*., 2022; Fleishman and Kumar, 2024). Curcumin reduces the inflammatory response and significantly improves liver tissue symptoms, thereby improving liver function in cholestasis rats (Frozandeh *et al*., 2021). Moreover,

**Corresponding author:* e-mail: xiaxia1199975353@126.com
#The authors contributed equally therefore they are the co-first authors.

curcumin shows promising potential for improving inflammatory bowel disease. It can ameliorate metabolic disorders of the intestinal-liver axis and restore gut microbiota composition (Zhu and He, 2024). Additionally, studies have shown that in mouse experiments, curcumin can reduce the expression of Keap1 and activate the downstream ARE signaling pathway, thereby exerting a protective effect against hepatocellular carcinoma and liver injury associated with abnormal bile acid metabolism (Liao *et al*., 2023) These studies fully demonstrate that, curcumin has a positive effect in inhibiting the development of liver cancer and preventing and treating bile acid enterohepatic circulation. However, whether it exerts these effects through the regulation of the STAT3 signaling pathway remains unclear and requires further investigation.

Therefore, this study aims to evaluate the effects of curcumin on the STAT3 signaling pathway and on bile acid enterohepatic circulation in mice with hepatocellular carcinoma. It also seeks to explore whether STAT3 regulation simultaneously mediates both anti-tumor effects and improvements in bile acid circulation, thereby providing new strategies and insights for the treatment of hepatocellular carcinoma.

MATERIALS AND METHODS

Main materials and instruments

All abbreviations used in this manuscript are defined in Table 1. Curcumin (purity: >98%, batch number: N1306, Sichuan Hengcheng Zhiyuan Biotechnology; The root extract of turmeric has antioxidant, anti-inflammatory, blood lipid lowering and other pharmacological effects and can also prevent and treat tumor-related diseases to a certain extent); STAT3 kit (Shanghai Xinyu Biotechnology); GAPDH (purity: >95%, batch number: PA1000-1196, Hubei Apti Biotechnology); PCR primers and kits (Shanghai Kolaman Reagent); RNA extraction kits (Weifang Gene Biotechnology); Cisplatin injection (Batch No.: P4394, Shanghai Yuanye Biotechnology Co., Ltd.); S3I-201 (STAT3-specific inhibitor, Batch No.: HY-13814, MedChemExpress, USA).

Curcumin was prepared as a suspension in physiological saline containing 1% sodium carboxymethyl cellulose (CMC-Na) prior to use; cisplatin injection was diluted with physiological saline to the required concentration before use; S3I-201 was prepared in a 5% DMSO physiological saline solution and used immediately after preparation. All reagents were stored and used according to the manufacturer's instructions.

Method

Establishment and grouping of animal models

Male C57BL/6J mice, aged 6–8 weeks and weighing 20–25 g, were purchased from (please insert vendor name and license number, e.g., Beijing Vital River Laboratory Animal Technology Co., Ltd.). All mice were housed under specific pathogen-free conditions with a 12 h light/dark cycle and ad libitum access to standard chow and water. A total of 45 mice were selected for this study. Among them, five mice were assigned to the sham surgery group (Sham group), which underwent only simulated procedures without tumor cell inoculation. The remaining 40 mice were used to establish a hepatocellular carcinoma model via intrahepatic injection of 10^6 Hepa1-6 cells. On day 10 after inoculation, high-frequency ultrasound was performed to observe tumor formation at the intraliver inoculation site. During the modeling process, 5 mice died, leaving 35 mice with successfully established models. The criteria for successful modeling (Cahyani *et al*., 2021) were as follows: ultrasound examination showed an intrahepatic space-occupying lesion with a diameter $\geqslant$ 3 mm; serum AFP levels were significantly higher than those in the Sham group ($P < 0.05$).

The mice with successfully established models were randomly divided into the following seven groups, with five mice in each group: Model control group (NC group): administered physiological saline daily by gavage; Curcumin low-dose group (Cur-L group): administered curcumin (10 mg/kg) daily by gavage; Curcumin medium-dose group (Cur-M group): administered curcumin (30 mg/kg) daily by gavage; Curcumin high-dose group (Cur-H group): administered curcumin (50 mg/kg) daily by gavage; STAT3 inhibitor group (S3I-201 group): administered S3I-201 (10 mg/kg) intraperitoneally once daily; Combined intervention group (Cur+S3I-201 group): administered curcumin (50 mg/kg) by gavage + S3I-201 (10 mg/kg) intraperitoneally once daily; Cisplatin positive control group (Cisplatin group): administered cisplatin (5 mg/kg) intraperitoneally daily following an intermittent dosing regimen, i.e., five consecutive days of administration followed by two days off, for a total of two treatment cycles (10 doses in total). The sham surgery group was administered an equivalent volume of physiological saline daily by gavage. All drug treatments were continued for two weeks. S3I-201 was freshly prepared in physiological saline containing 5% DMSO before use and cisplatin was freshly prepared in physiological saline before use.

Sample size (n = 5 per group) was determined based on a pilot experiment showing a 50% reduction in p-STAT3 levels, with $\alpha = 0.05$ and power = 0.80 using G*Power software (version 3.1).

All outcome assessments (histology, Western blot, qRT-PCR, serum biochemistry) were performed by investigators blinded to group allocation. Animal care and gavage administration were performed by separate personnel.

HE staining to examine the pathological morphology of the mouse liver tissue

After euthanasia, liver tissues were collected from the mice and fixed in 4% paraformaldehyde for 24 hours. The

tissues were then dehydrated through a graded ethanol series, cleared in xylene, embedded in paraffin and sectioned into slices (4 μm thick). The sections were deparaffinized in xylene, rehydrated through a graded ethanol series and sequentially stained by immersion in Harris hematoxylin for 5–8 minutes, differentiated in 1% acid alcohol and blued in running water. This was followed by counterstaining with 0.5% eosin for 1–3 minutes. Finally, the sections were dehydrated in ethanol, cleared in xylene, mounted with neutral balsam and observed under an optical microscope (Olympus BX53) for image acquisition to evaluate pathological changes, including hepatocellular morphology, structural arrangement, nuclear atypia and inflammatory infiltration.

Serum biochemical testing and IL-6 and TGF-β1 level determination

After the mice were sacrificed, blood was collected, the serum separated and stored at -80ºC in a refrigerator, then thawed at 4ºC before use. ELISA was then performed according to the manufacturer's instructions and IL-6 and TGF-β1 levels were detected.

Western blot detection of STAT3 pathway protein in liver tissue

Approximately 50 mg of liver tissue from each group of mice was taken and homogenized on ice with RIPA lysis buffer (containing protease and phosphatase inhibitors). After centrifugation at 4ºC, the supernatant was collected. Protein concentration was determined using the BCA method. Equal amounts of protein samples (30 μg) were separated by 10% SDS-PAGE electrophoresis (120 V, 100 min) and then transferred to a PVDF membrane via wet transfer (200 mA, 90 min). Following blocking with 5% skim milk at room temperature for 2 hours, the membranes were incubated overnight at 4ºC with the following primary antibodies: p-STAT3 (Tyr705) (rabbit monoclonal, CST #9145, 1:1000), total STAT3 (rabbit monoclonal, CST #12640, 1:1000), Bcl-2 (rabbit monoclonal, CST #3498, 1:1000), Cyclin D1 (rabbit monoclonal, CST #2978, 1:1000), BSEP (rabbit polyclonal, Abcam #ab111016, 1:500), NTCP (rabbit polyclonal, Santa Cruz #sc-271232, 1:500), FXR (rabbit monoclonal, Abcam #ab197701, 1:1000) and GAPDH (mouse monoclonal, Proteintech #60004-1-Ig, 1:5000).

The next day, after washing three times with TBST (10 min each), the membranes were incubated with corresponding horseradish peroxidase-conjugated secondary antibodies (goat anti-rabbit/anti-mouse, 1:10000) at room temperature for 1 hour. Protein bands were visualized using ECL chemiluminescence reagent and band grayscale values were analyzed with ImageJ software. The STAT3 activation level was expressed as the ratio of p-STAT3 to total STAT3, while the expression of other proteins was normalized to GAPDH as an internal reference. All experiments were independently repeated three times.

qRT-PCR detection

Total RNA was extracted from liver tissue using the TRIzol method and its concentration and purity were measured using a NanoDrop. One microgram of RNA was reverse-transcribed into cDNA using the PrimeScript RT reagent kit. Amplification was performed on the QuantStudio 5 system using the SYBR Green method, with a reaction volume of 20 μL containing TB Green Premix, primers and cDNA template. The primer sequences covered STAT3, BSEP, NTCP, FXR, FGF15/19 and the internal reference GAPDH. The reaction program consisted of an initial denaturation at 95ºC for 30 seconds, followed by 40 cycles of 95ºC for 5 seconds and 60ºC for 30 seconds and concluded with melt curve analysis. The relative gene expression levels were calculated using the $2^{-\Delta\Delta Ct}$ method, with three replicate wells per sample and three independent experimental repetitions. Table 2 lists the primers and primer sequences.

Detection of ALT, AST and other indicators

A syringe was used to collect blood from the mouse's heart or abdominal aorta, which was then placed in a centrifuge tube containing heparin anticoagulant and gently mixed. The samples were centrifuged for 10 min and serum was separated. The instructions for the ALT detection kit and the AST detection kit were followed by mixing the buffer and samples evenly, then adding the ALT and AST enzyme activity detection reagents, respectively. The samples were shaken gently to mix and let to stand for 10 minutes. Spectrophotometry was used to measure the absorbance value of each tube with a meter and record the data.

Statistical analysis

All data were processed and analyzed using GraphPad Prism 8.0.2 and the F test was used, with $P<0.05$ as the criterion for significance. One-way analysis of variance (ANOVA) followed by Tukey‘s post-hoc test for multiple comparisons was used. A P-value < 0.05 was considered statistically significant.

RESULTS

Successful construction of liver cancer mouse model

compared with the sham group, the livers of mice in the NC group were enlarged, dark red in color, hard in texture and had gray-white spot-like pigmentation (Fig. 1). Dynamic monitoring via high-frequency ultrasound revealed that mice in the NC group showed small intrahepatic space-occupying lesions on day 10 after inoculation (volume: 15.2 ± 3.8 mm^3), while no space-occupying lesions were observed in the Sham group. Simultaneously, on day 10 after inoculation, the serum AFP level in the NC group was 85.6 ± 12.3 ng/mL, which was significantly higher than that in the Sham group (12.5 ± 3.2 ng/mL, $P = 0.001$). During the two-week treatment period, no treatment-related mortality or visible adverse events (e.g., diarrhea, body weight loss > 20%, reduced activity, or abnormal behavior) were observed in any of the curcumin, S3I-201, or combination intervention groups.

Table 1: List of abbreviations

Abbreviation	Full name
STAT3	Signal transducer and activator of transcription 3
ALT	Alanine aminotransferase
AST	Aspartate aminotransferase
TB	Total bilirubin
TBA	Total bile acids
BSEP	Bile salt export pump
NTCP	Na+-taurocholate cotransporting polypeptide
FXR	Farnesoid X receptor
FGF15/19	Fibroblast growth factor 15/19
Cyp7a1	Cytochrome P450 family 7 subfamily A member 1
Shp	Small heterodimer partner
Asbt	Apical sodium-dependent bile acid transporter
ELISA	Enzyme-linked immunosorbent assay
qRT-PCR	Quantitative real-time reverse transcription polymerase chain reaction
WB	Western blot

Table 2: Real-time PCR primers and primer sequences.

Primer		Sequences
STAT3	Forward primer	5'-TGGAGAAGGCTCCTGGTGA-3'
	Reverse primer	5'-TCTGGAGGACTTCTCCAGG-3'
Bcl-2	Forward primer	5'-GCTACCGTCGTGACTTCGC-3'
	Reverse primer	5'-CCCCACCGAACTCAAAGAAGG-3'
Cyclin D1	Forward primer	5'-GCGTACCCTGACACCAATCTC-3'
	Reverse primer	5'-CTCCTCTTCGCACTTCTGCTC-3'
c-Myc	Forward primer	5'-TGAGGAGACACCGCCCAC-3'
	Reverse primer	5'-CAACATAGGATGGAGAGCGAA-3'
VEGF	Forward primer	5'-GCACATAGAGAGAATGAGCTTCC-3'
	Reverse primer	5'-CTCCGCTCTGAACAAGGCT-3'
Cyp7a1	Forward primer	5'-CTTCCAGAGAGCCATCATTGC-3'
	Reverse primer	5'-AGTAGGGAGCGGATGAAGGT-3'
Shp	Forward primer	5'-AGACGCCTTCAAGCCCTAC-3'
	Reverse primer	5'-GCTGATGTCCATGGCAAAGA-3'
FGF15	Forward primer	5'-CAGGACTTCGACAGCACCAT-3'
	Reverse primer	5'-GTCCTCCTTGGTGGTCATCA-3'
Asbt	Forward primer	5'-TGGCATTGTCACTGGTGTTG-3'
	Reverse primer	5'-CAGAGCAGGTTGGCATAGGA-3'
GAPDH	Forward primer	5'-AAAGGGTCATCATCTCCGCC-3'
	Reverse primer	5'-AGTGATGGCATGGACTGTGG-3'

Effect of curcumin on pathological morphology of mouse liver tissue

The HE staining results showed that curcumin dose-dependently improved the pathological morphology of the liver in hepatocellular carcinoma mice. In the sham-surgery group, the hepatic lobular structure was normal. In the model group, the liver tissue structure was severely disrupted, with extensive proliferation of atypical tumor cells, polymorphic and hyperchromatic nuclei, widespread apoptotic and necrotic changes and inflammatory infiltration. In the cisplatin group, the tumor area was reduced, apoptotic cells increased and the structure was partially restored. The improvement effects in the low-, medium- and high-dose curcumin groups increased progressively, with the high-dose group showing the most significant effects, including markedly restored liver tissue integrity, minimal tumor cell presence, nearly normal hepatocellular morphology and arrangement and essentially absent apoptotic necrosis and inflammation (Fig. 2).

Curcumin inhibits activation of the STAT3 signaling pathway in mice with liver cancer and improve enterohepatic circulation of bile acids

Western blot analysis showed that p-STAT3 (Tyr705) expression in liver tissues of the NC group mice was significantly increased (3.2-fold higher than in the Sham group, $P < 0.001$). In contrast, total STAT3 protein levels did not change significantly. Curcumin intervention dose-dependently inhibited p-STAT3 levels, with the p-

STAT3/total STAT3 ratio in the Cur-H group reduced by 68% compared to the NC group ($P < 0.001$), an effect comparable to that of the Cisplatin group. In the NC group, the protein expression levels of Bcl-2 and Cyclin D1 were significantly upregulated (increased by 2.8-fold and 3.1-fold, respectively). All curcumin dose groups downregulated the expression of these target proteins, with the most pronounced effect observed in the Cur-H group (55–70% reduction compared to the NC group, $P < 0.01$) (Fig. 3A). qPCR results indicated that mRNA expression levels of Bcl-2, Cyclin D1, c-Myc and VEGF were significantly elevated in the NC group. After curcumin intervention, the expression of these genes decreased dose-dependently, with the Cur-H group nearly restoring them to normal levels (Fig. 3B).

The results from mouse experiments showed that the levels of serum ALT, AST, TB and TBA in the NC group were significantly increased (P<0.001), suggesting liver injury and a disorder of bile acid metabolism. Curcumin intervention improved these indicators in a dose-dependent manner. The effect was most significant in the Cur-H group, approaching the level of the cisplatin positive control group. After curcumin intervention, these indicators decreased in a dose-dependent manner and the Cur-H group approached normal levels (Table 3). At the same time, compared with the Cisplatin group, the expressions of BSEP, NTCP and FXR in the curcumin intervention group were significantly increased (Figs. 3C-3E). The expression of FGF15/19 was decreased (Fig. 3F). To further elucidate the regulatory effect of curcumin on bile acid synthesis and feedback, qPCR results showed (Fig. 3G) that compared with the Sham group, the mRNA expression of Cyp7a1, the rate-limiting enzyme for bile acid synthesis in the liver of the NC group mice, was significantly upregulated (5.20 ± 0.75 fold, $P < 0.01$), while the expression of Shp, a direct downstream target gene of FXR and a negative feedback regulator, was suppressed to 30% ($P < 0.01$).

Curcumin intervention dose-dependently reversed these changes: the Cur-H group suppressed Cyp7a1 expression to 1.30 ± 0.25 fold and elevated Shp expression to 1.10 ± 0.18 fold (both $P < 0.01$ vs. NC group). Furthermore, in ileal tissue, the mRNA expression of Fgf15 and Asbt was also significantly reduced in the NC group. Curcumin treatment, especially at medium and high doses, effectively upregulated the expression of both (Cur-H group restored to 1.30 ± 0.20-fold and 1.25 ± 0.22-fold, respectively; $P < 0.01$).

Effects of curcumin on enterohepatic circulation of bile acids in mice with liver cancer by inhibiting STAT3 signaling

In mouse studies, we found that differences in serum levels of ALT, AST, TB and TBA were significant under the combined intervention of Cur and S3I-201, $p < 0.05$ (Table 4). The relative expression of STAT3 decreased significantly under the combined intervention by Cur and S3I-201 (Fig. 4A). At the same time, there were significant differences in HE-stained sections of mouse livers under combined Cur and S3I-201 intervention (Fig. 4B). S3I-201 monotherapy can partially improve liver function, slightly upregulate FXR, BSEP and NTCP and reduce FGF15/19, but its effect is weaker than that of the Cur-H group. The combination of Cur-H and S3I-201 did not show a significantly better synergistic effect than curcumin monotherapy (Figs. 4C-4F).

DISCUSSION

This study established a mouse model of liver cancer, by giving mice different doses of curcumin and tested the pathological morphology of liver tissue and serum from mice with liver cancer. It was found that, compared with low-dose curcumin, high-dose curcumin improved the morphology of liver tissue cells. It also had a more significant effect on reducing serum ALT, AST, TB and TBA levels, as well as the inflammatory factors IL-6 and TGF-β1 and on increasing BSEP, NTCP and FXR. At the same time, this study found that curcumin upregulated the expression of the gut-derived hormone FGF15. FGF15/19 is an enterohepatic axis signaling molecule produced upon intestinal FXR activation and its role is to inhibit excessive bile acid synthesis in the liver (Tian *et al*., 2023). The downregulation of Fgf15 in the NC group may be related to intestinal dysfunction or insufficient intestinal FXR activation. The upregulatory effect of curcumin on Fgf15 suggests that it may also act at the intestinal level, improving enterohepatic feedback regulation by modulating intestinal FXR or directly protecting intestinal epithelial function. This aligns with the known intestinal anti-inflammatory and barrier-protective functions of curcumin (Guo *et al*., 2022, Cao *et al*., 2022). In addition, curcumin can significantly reduce ALT and AST levels. This shows that curcumin can reduce liver damage and inflammation, restore bile acid synthesis and normalize bile acid transport and excretion, thereby improving enterohepatic circulation of bile acids. High-dose curcumin was more effective than low-dose curcumin. This is because curcumin can inhibit NF-κB signaling (Zoi *et al*., 2021; Ran *et al*., 2021), thereby reducing the production of TNF-α, IL-6 and also inflammation such as COX-2 (Gouthamchandra *et al*., 2021, Eldesoqui *et al*., 2025) and iNOS gene expression, inhibiting the development of liver cancer. It can also promote bile acid synthesis by activating the FXR signaling pathway (Meshanni *et al*., 2024), increasing bile acid uptake and transport in the liver and inhibiting intestinal reabsorption of bile acids. At the same time, it can promote bile acid synthesis by activating the PXR signaling pathway (Tian *et al*., 2023). The expression and activity of the CYP3A enzyme are beneficial for bile acid metabolism and excretion, thereby improving enterohepatic circulation.

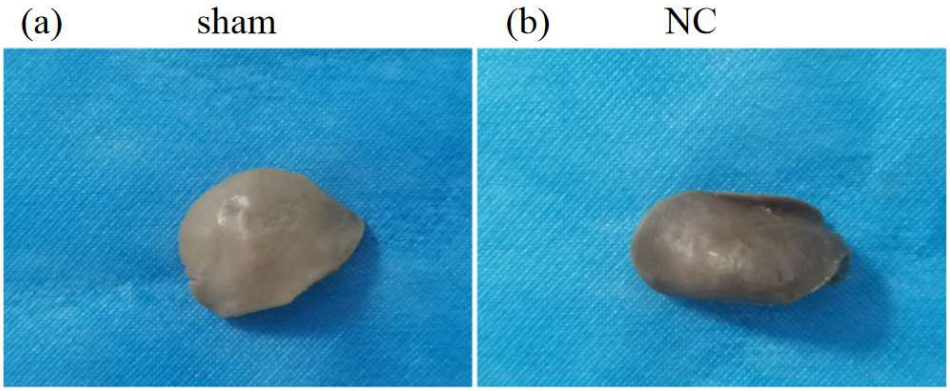

Fig. 1: Successful construction of mouse model of liver cancer.
Note: (a) Sham group – normal liver size, smooth surface, uniform reddish-brown color; (b) Model control (NC) group – enlarged liver, dark red color, hard texture, with gray-white spotted pigmentation. Abbreviations: NC, model control group.

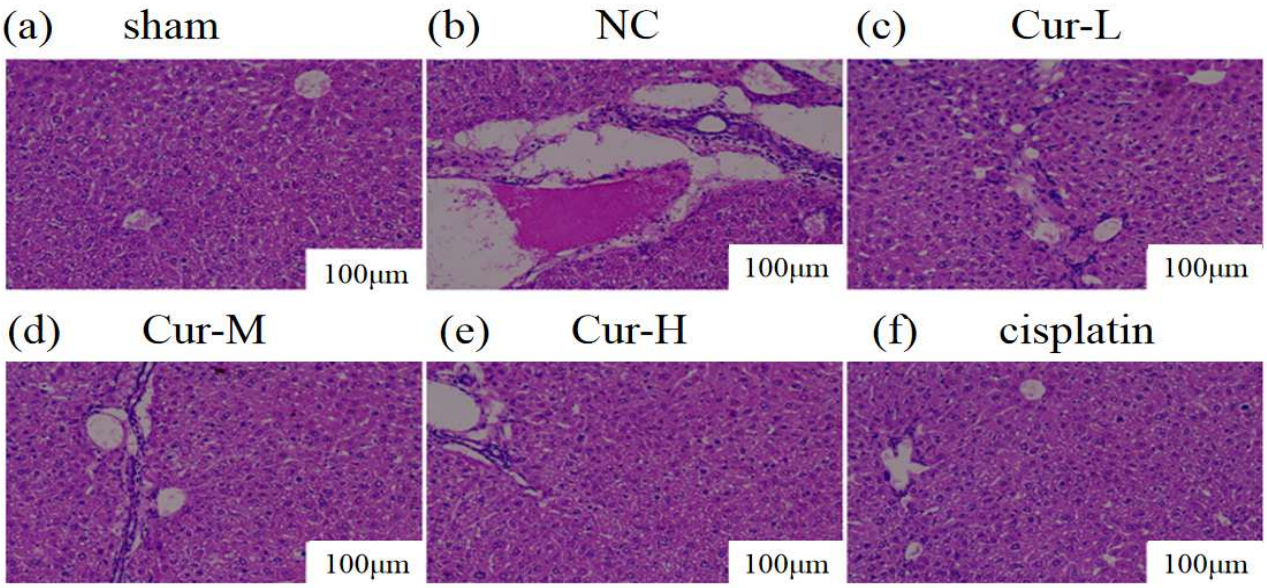

Fig. 2: Effect of curcumin on liver histopathological morphology of mice.
Note: Representative hematoxylin and eosin (HE) staining images of liver tissue sections from each group (original magnification: 200×; scale bar = 100 μm). (a) Sham group: Normal hepatic lobular architecture, with hepatocytes arranged in regular cords around the central vein. No evidence of necrosis, apoptosis, or inflammatory infiltration; (b) Model control (NC) group: Severe disruption of liver tissue structure, with extensive proliferation of atypical tumor cells (indicated by black arrows). Hepatocytes show marked nuclear pleomorphism, hyperchromasia, and increased nuclear-to-cytoplasmic ratio. Widespread apoptotic bodies (yellow arrowheads) and necrotic areas (asterisks) are observed, accompanied by dense inflammatory cell infiltration; (c) Curcumin low-dose (Cur-L) group: Moderate improvement compared to the NC group. Tumor cell proliferation is reduced but still evident. Apoptotic and necrotic changes are partially alleviated, with residual inflammatory infiltration; (d) Curcumin medium-dose (Cur-M) group: Marked improvement. Liver tissue integrity is partially restored. Tumor cells are scattered rather than confluent. Apoptosis and necrosis are significantly reduced, with only mild inflammation; (e) Curcumin high-dose (Cur-H) group: Most significant improvement among curcumin-treated groups. Liver tissue structure is nearly normal, with minimal residual tumor cells. Hepatocellular morphology and cord-like arrangement are largely restored. Apoptotic necrosis and inflammatory infiltration are essentially absent; (f) Cisplatin group: The tumor area is markedly reduced, with increased apoptotic cells (yellow arrowheads) and partially restored lobular architecture, comparable to the Cur-H group.Abbreviations: HE, hematoxylin and eosin; NC, model control group; Cur-L, curcumin low-dose (10 mg/kg); Cur-M, curcumin medium-dose (30 mg/kg); Cur-H, curcumin high-dose (50 mg/kg); μm, micrometers.

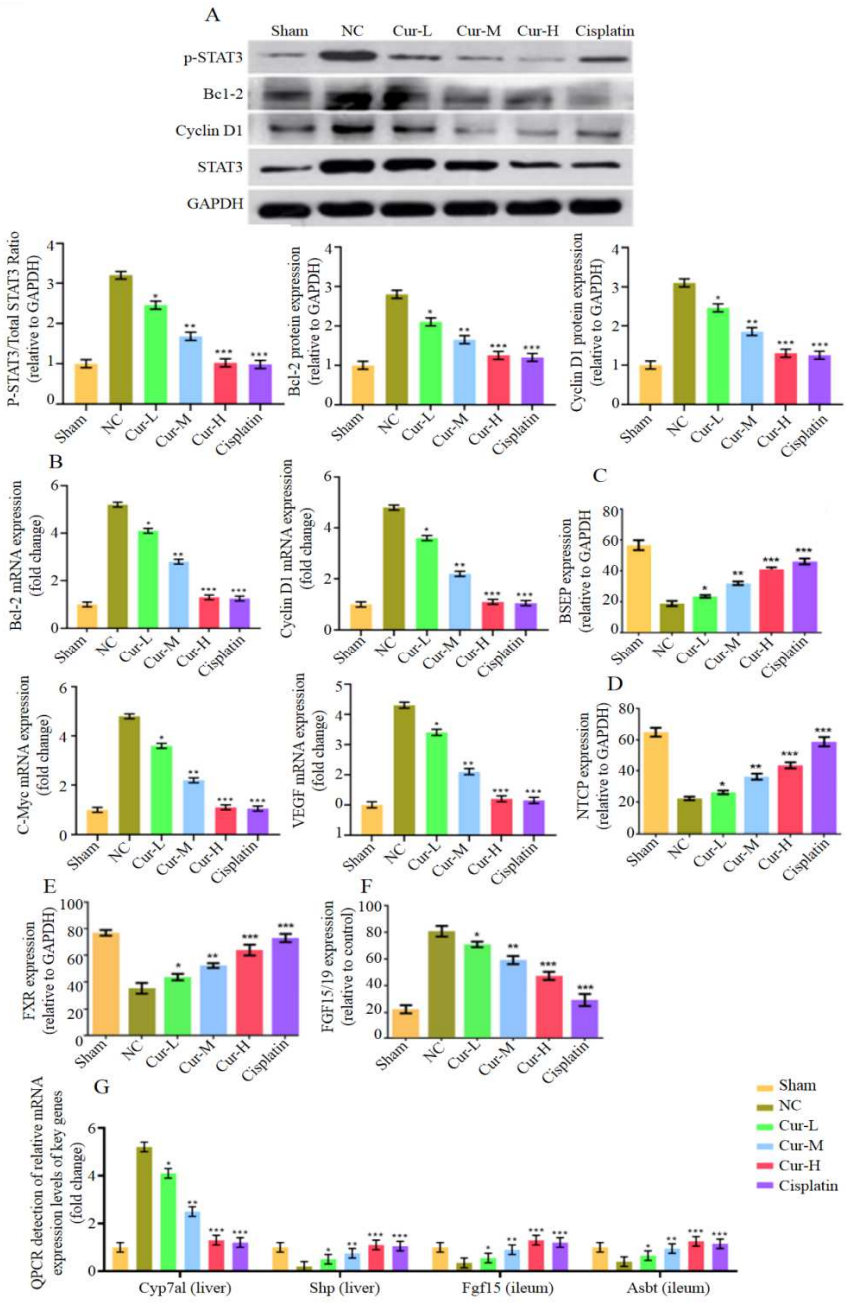

Fig. 3: Activation of the STAT3 signaling pathway in each group.

Note: (A) Representative Western blot bands (upper panel) and quantitative bar charts (lower panel) showing protein expression levels of p-STAT3, Bcl-2 and Cyclin D1 in liver tissues of each group. GAPDH was used as the loading control. The p-STAT3/total STAT3 ratio was calculated to indicate STAT3 activation. Data are presented as mean ± SD (n = 3 independent experiments).; (B) qRT-PCR analysis of mRNA expression levels of STAT3 downstream target genes: Bcl-2, Cyclin D1, c-Myc, and VEGF in liver tissues. Relative expression was normalized to GAPDH using the 2^−ΔΔCt^ method.; (C)Quantitative comparison of BSEP protein expression (normalized to GAPDH); (D) uantitative comparison of NTCP protein expression (normalized to GAPDH); (E) Quantitative comparison of FXR protein expression (normalized to GAPDH).; (F) qRT-PCR analysis of FGF15/19 mRNA expression in ileal tissues; (G) qRT-PCR analysis of key bile acid metabolism regulators: Cyp7a1 (rate-limiting enzyme for bile acid synthesis) and Shp (negative feedback regulator) in liver tissues; Fgf15 (ileal-derived feedback hormone) and Asbt (apical sodium-dependent bile acid transporter) in ileal tissues. Abbreviations: NC, model control group; Cur-L, curcumin low-dose (10 mg/kg); Cur-M, curcumin medium-dose (30 mg/kg); Cur-H, curcumin high-dose (50 mg/kg); Cis, cisplatin group. *P < 0.05, **P < 0.01, ***P < 0.001 compared with the NC group. All experiments were repeated three times independently.

Table 3: Serum ALT, AST, TB and TBA levels of mice in each group (x±s).

Group	N	ALT (U/L)	AST (U/L)	TB (μmol/L)	TBA (μmol/L)
Sham group	12	42.65±10.25	120.58±19.44	6.78±0.15	60.25±12.45
NC group	12	254.55±56.14	542.01±71.28	42.98±8.21	144.22±26.31
Curcumin low dose group	12	186.78±36.16	413.25±50.24	32.04±6.01	117.38±21.08
Curcumin medium dose group	12	118.24±25.36	274.89±36.98	18.64±4.12	88.65±17.24
Curcumin high dose group	12	47.98±10.68	135.24±24.12	7.91±1.36	64.21±12.77
Cisplatin group	12	45.98±8.65	125.12±22.15	8.14±1.02	64.12±14.21
F value	-	83.981	155.501	95.765	28.186
P value	-	0.000	0.000	0.000	0.000

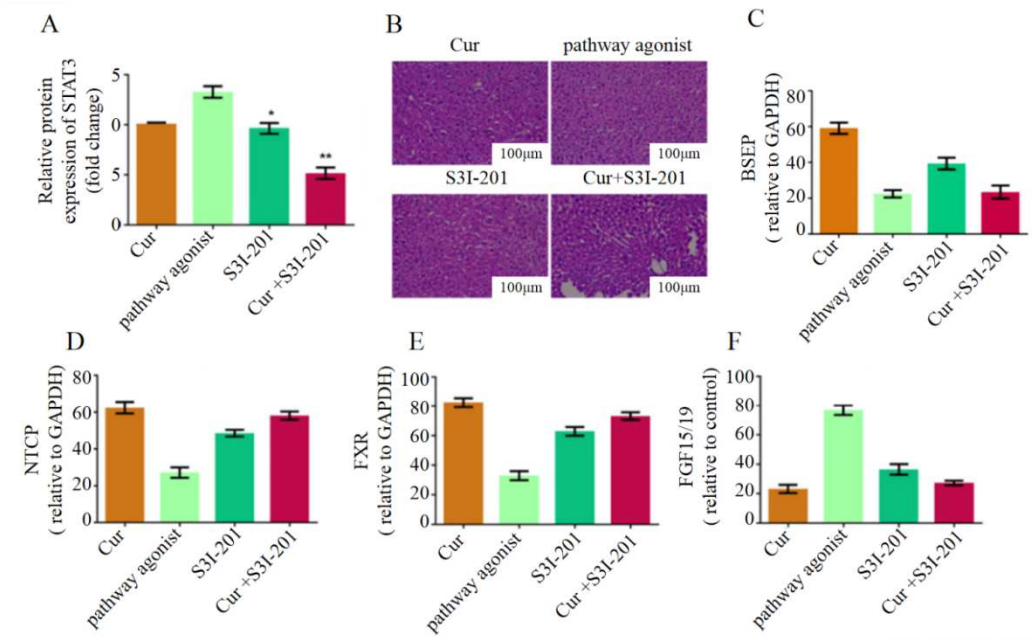

Fig. 4: Effect of STAT3 signaling on bile acid enterohepatic circulation in liver cancer mice.
Note: (A) Quantitative bar chart showing STAT3 total protein expression levels in liver tissues of each group, as measured by Western blot. GAPDH was used as the loading control. Data are presented as mean ± SD (n = 3 independent experiments); (B) Representative HE staining images of liver tissue sections from each group (original magnification: 200×; scale bar = 100 μm): Cur group (Curcumin group): Liver tissue structure is nearly normal, with minimal residual tumor cells (black arrows). Hepatocellular morphology and cord-like arrangement are largely restored. Apoptotic necrosis and inflammatory infiltration are essentially absent. Pathway agonist group: Severe disruption of liver tissue structure, with extensive proliferation of atypical tumor cells (black arrows). Hepatocytes show marked nuclear pleomorphism, hyperchromasia and increased nuclear-to-cytoplasmic ratio. Widespread apoptotic bodies (yellow arrowheads) and necrotic areas (asterisks) are observed, accompanied by dense inflammatory cell infiltration. S3I-201 group (STAT3 inhibitor group): The tumor area is markedly reduced, with increased apoptotic cells (yellow arrowheads) and partially restored lobular architecture, comparable to the Cur-H group.Cur+S3I-201 group (Combined intervention group): Liver tissue integrity is further restored, with very few residual tumor cells. Apoptotic necrosis and inflammatory infiltration are essentially absent; (C) Quantitative comparison of BSEP (bile salt export pump) protein expression in liver tissues of each group (normalized to GAPDH); (D) Quantitative comparison of NTCP (Na^+-taurocholate cotransporting polypeptide) protein expression in liver tissues of each group (normalized to GAPDH); (E) Quantitative comparison of FXR (farnesoid X receptor) protein expression in liver tissues of each group (normalized to GAPDH); (F) qRT-PCR analysis of FGF15/19 (fibroblast growth factor 15/19) mRNA expression in ileal tissues of each group. Relative expression was normalized to GAPDH using the 2^−ΔΔCt^ method. Abbreviations: Cur, curcumin; NC, model control group; S3I-201, STAT3-specific inhibitor; HE, hematoxylin and eosin; STAT3, signal transducer and activator of transcription 3; BSEP, bile salt export pump; NTCP, Na^+-taurocholate cotransporting polypeptide; FXR, farnesoid X receptor; FGF15/19, fibroblast growth factor 15/19; GAPDH, glyceraldehyde-3-phosphate dehydrogenase; qRT-PCR, quantitative real-time reverse transcription polymerase chain reaction; SD, standard deviation; μm, micrometer.*P < 0.05, **P < 0.01, ***P < 0.001 (compared with the NC group). All experiments were independently repeated three times.t

Table 4: Serum ALT, AST, TB and TBA levels of mice in each group (x±s).

Group	n	ALT (U/L)	AST (U/L)	TB (μmol/L)	TBA (μmol/L)
Cur group	12	49.65±8.18	138.24±10.25	8.24±1.05	72.21±11.74
Pathway agonist group	12	254.21±50.24	583.12±46.72	49.65±6.77	156.57±23.07
S3I-201 group	12	44.57±2.14	130.24±22.71	7.23±1.12	61.12±11.54
Cur+S3I-201 group	12	42.68±8.29	121.35±10.89	7.87±0.65	60.28±10.05
F value	-	3.336	3.476	3.382	4.291
P value	-	0.048	0.043	0.046	0.022

A previous study on liver injury (Li *et al*., 2021) found that curcumin can reduce ALT and AST activities and lower TBIL and TBA levels, thereby alleviating liver damage. Meanwhile, the data from this study show that curcumin significantly upregulates FXR and its downstream effector molecules in the livers of hepatocellular carcinoma model mice. The activation of FXR triggers a synergistic adaptive response. On the one hand, it upregulates the bile salt export pump (BSEP), facilitating the excretion of intrahepatic bile acids into the bile ducts (Dai *et al*., 2023); on the other hand, it downregulates the basolateral uptake transporter NTCP, reducing the reuptake of bile acids from the portal blood (Wang *et al*., 2025). Additionally, it induces SHP expression, which in turn inhibits the transcription factor LRH-1, ultimately leading to downregulation of the rate-limiting enzyme for bile acid synthesis, CYP7A1 (Choi *et al*., 2022). The downregulation of Cyp7a1 and upregulation of Shp observed in this study are entirely consistent with this classic pathway. Furthermore, curcumin also upregulates intestinal Fgf15, which, upon entering the liver, cooperatively inhibits CYP7A1 through the FGFR4/β-Klotho signaling pathway (Lvova *et al*., 2023). Therefore, by synergistically activating the FXR signaling pathway in both the liver and intestine, curcumin alleviates the hepatic bile acid load through multiple mechanisms.

Furthermore, a complete enterohepatic circulation involves efficient intestinal reabsorption and hepatic portal uptake of bile acids. Under pathological conditions, maintaining an appropriate level of intestinal reabsorption is necessary to preserve the total bile acid pool. This study found that under curcumin intervention, intestinal Asbt expression was moderately upregulated, suggesting a compensatory or protective response aimed at reducing excessive bile acid loss in feces. However, given the more potent dominant changes such as downregulation of hepatic NTCP, upregulation of BSEP and reduced synthesis of CYP7A1, the net effect of curcumin is to promote bile acid flow from the liver into the intestine and its subsequent elimination, rather than simply increasing its accumulation in the liver. This helps to break the vicious cycle of bile acid stasis and inflammation/injury within the hepatocellular carcinoma microenvironment. To explore the effects of the STAT3 signaling pathway on liver cancer and bile acid enterohepatic circulation in mice, we examined liver tissue sections from mice under STAT3 pathway stimulation and inhibition and from mice treated with curcumin. In contrast, due to the influence of STAT3 pathway agonists, the boundaries between liver cells were blurred and the tissue structure was chaotic; the nuclei of cancer cells were of different shapes and sizes, showing different shades after staining and mitosis was abnormally active in STAT3. This phenomenon was significantly improved with intervention using pathway inhibitors and after adding curcumin, the improvement effect was further strengthened. Serum ALT, AST, TB, TBA and FGF15/19 expression levels decreased at the same time, while BSEP, NTCP and FXR expressions increased which suggests that curcumin may indirectly restore bile acid homeostasis by antagonizing STAT3-driven inflammation and relieving its inhibition of the FXR pathway. However, the use of the STAT3-specific inhibitor S3I-201 can only partially mimic the effect of curcumin and the combination therapy does not show a significant increase in efficacy, indicating that STAT3 inhibition is an important but not the only mechanism by which curcumin acts.

The doses of curcumin selected in this study (10–50 mg/kg) have been demonstrated to exhibit anti-inflammatory and anti-tumor activities in multiple mouse disease models (Xu *et al*., 2021; Fontes *et al*., 2022). The oral bioavailability of curcumin is notably low (Tabanelli *et al*., 2021). This study did not directly measure curcumin or its active metabolites in the mice. Therefore, the systemic effects observed in this study may be partly attributable to local actions of curcumin in the intestine, such as modulating the gut microbiota, enhancing barrier function, regulating the activity of metabolites, or indirect regulation mediated by the gut-liver axis (Lamichhane *et al*., 2024, Hong *et al*., 2022). This study has the following limitations: the experiments were conducted only in a mouse model and caution is required when extrapolating the results to humans; the actual exposure levels of curcumin and its metabolites *in-vivo* were not measured and thus the direct relationship between bioavailability and efficacy remains unclear; furthermore, the study focused on the STAT3 pathway and bile acid circulation, while mechanisms involving other signaling networks through which curcumin may exert effects were not fully explored. Future research should incorporate clinical samples, pharmacokinetic studies and multi-omics technologies for further validation and mechanistic investigation.

CONCLUSION

In summary, curcumin can reduce liver damage by inhibiting STAT3 signaling, increasing bile acid

reabsorption in the liver and improving bile acid utilization efficiency, thereby alleviating the vicious cycle of bile acids. This study broadens the research field of anti-liver cancer mechanisms. By studying the mechanism of curcumin on liver cancer, we can further explore the role of bile acid enterohepatic circulation in liver cancer and its regulatory mechanism, which will help reveal liver cancer pathogenesis and provide new insights into the treatment and prevention of liver cancer. However, these findings were derived only from a mouse model. Therefore, further experimental data are needed to confirm its efficacy and safety.

Acknowledgments
This work was supported by the Shanxi Provincial Administration of Traditional Chinese Medicine (No.2023ZYYDA2002); The first "One Outline and Two Objectives" miscellaneous disease academic school of the Three Jin Dynasties in Shanxi Province, National Hu Lan Gui Famous Traditional Chinese Medicine Studio.

Authors' contributions
Langui Hu: Experimental design, data collection and analysis and thesis writing; Tingting Zhao: Experimental operation and data processing; Niu Yan: Research guidance, paper revision and review; Na Hu: Material provision and technical support. All authors have read and agreed to the final manuscript.

Funding
There was no funding.

Data availability statement
Data are available from the corresponding author upon reasonable request.

Ethical approval
All animal experiments in this study were conducted in accordance with the guidelines for the care and use of laboratory animals approved by the Ethics Committee of the School of Pharmacy, Guangdong Medical University (Approval Number: GXC2025089). This study was performed in adherence with the ARRIVE guidelines. See supplementary file for the ARRIVE checklist.

Conflicts of interest
The author states that this research was conducted without any commercial or financial interests that could be interpreted as potential conflicts of interest. There are no conflicts to declare.

Supplementary data
https://www.pjps.pk/uploads/2026/05/SUP1778927132.pdf

REFERENCES

Cahyani DM, Miatmoko A, Hariawan BS, Purwantari KE and Sari R (2021). N-nitrosodiethylamine induces inflammation of liver in mice. *J Basic Clin Physiol Pharmacol*., **32**(4): 505–510.

Cui ZY, Wang G, Zhang J, Song J, Jiang YC, Dou JY, Lian LH, Nan JX and Wu YL (2021). Parthenolide, bioactive compound of *Chrysanthemum parthenium* L., ameliorates fibrogenesis and inflammation in hepatic fibrosis via regulating the crosstalk of TLR4 and STAT3 signaling pathway. *Phytother Res*., **35**(10): 5680-5693.

Cao Z, Gao J, Huang W, Yan J, Shan A and Gao X (2022). Curcumin mitigates deoxynivalenol-induced intestinal epithelial barrier disruption by regulating Nrf2/p53 and NF-κB/MLCK signaling in mice. *Food Chem Toxicol.,* **167**: 113281.

Choi YJ, Yang HS, Zhang Y, Lee W, Yun SH, Nam Y A, Lee G, Jung BH, Chang TS, Lee K and Lee BH (2022). Intratracheal exposure to polyhexamethylene guanidine phosphate disrupts coordinate regulation of FXR-SHP-mediated cholesterol and bile acid homeostasis in mouse liver. *Ecotoxicol Environ Saf*., **247**: 114213.

Dai Y, Jia Z, Fang C, Zhu M, Yan X, Zhang Y, Wu H, Feng M, Liu L, Huang B, Li Y, Liu J and Xiao H (2023). Polygoni Multiflori Radix interferes with bile acid metabolism homeostasis by inhibiting *Fxr* transcription, leading to cholestasis. *Front Pharmacol*., **14**: 1099935.

Eldesoqui M, Embaby EM, Fouad RA, Alrajhi YM, Mohammed ZA, Albadawi EA, Al-Serwi RH, El-Mansi AA, Hendawy M and Ahmed ME (2025). Curcumin attenuates malathion-induced lung injury in rats by modulating oxidative stress, inflammation and fibrosis via Nrf2/HO-1, NF-κB/TNF-α and COX-2 pathways. *Tissue Cell*., **98**: 103144.

Fleishman JS and Kumar S (2024). Bile acid metabolism and signaling in health and disease: Molecular mechanisms and therapeutic targets. *Signal Transduct Target Ther*., **9**(1): 97.

Fontes SS, Nogueira ML, Dias RB, Rocha CAG, Soares MBP, Vannier-Santos MA and Bezerra DP (2022). Combination therapy of curcumin and disulfiram synergistically inhibits the growth of B16-F10 melanoma cells by inducing oxidative stress. *Biomolecules.*,**12**(11):1600.

Frozandeh F, Shahrokhi N, Khaksari M, Amiresmaili S, AsadiKaram G, Shahrokhi N and Iranpour M (2021). Evaluation of the protective effect of curcumin on encephalopathy caused by intrahepatic and extrahepatic damage in male rats. *Iran J Basic Med Sci*., **24**(6): 760-766.

Ghufran H, Azam M, Mehmood A, Ashfaq R, Baig MT, Malik K, Shahid AA and Riazuddin S (2022). Tumoricidal effects of unprimed and curcumin-primed adipose-derived stem cells on human hepatoma HepG2 cells under oxidative conditions. *Tissue Cell*.,**79**:101968.

Girisa S, Saikia Q, Bordoloi D, Banik K, Monisha J, Daimary UD, Verma E, Ahn KS and Kunnumakkara AB (2021) Xanthohumol from Hop: Hope for cancer prevention and treatment. *IUBMB Life*., **73**(8):1016-1044.

Gouthamchandra K, Sudeep HV, Chandrappa S, Raj A, Naveen P and Shyamaprasad K (2021). Efficacy of a standardized turmeric extract comprised of 70% bisdemothoxy-curcumin (REVERC3) against LPS-induced inflammation in RAW264.7 cells and carrageenan-induced paw edema. *J Inflamm Res*., **14**: 859-868.

Guo X, Xu Y, Geng R, Qiu J and He X (2022). Curcumin alleviates dextran sulfate sodium-induced colitis in mice through regulating gut microbiota. *Mol Nutr Food Res*., **66**(8): e2100943.

Hong T, Jiang X, Zou J, Yang J, Zhang H, Mai H, Ling W and Feng D (2022). Hepatoprotective effect of curcumin against bisphenol A-induced hepatic steatosis via modulating gut microbiota dysbiosis and related gut-liver axis activation in CD-1 mice. *J Nutr Biochem*., **109**: 109103.

Lamichhane G, Olawale F, Liu J, Lee DY, Lee SJ, Chaffin N, Alake S, Lucas EA, Zhang G, Egan JM and Kim Y (2024). Curcumin mitigates gut dysbiosis and enhances gut barrier function to alleviate metabolic dysfunction in obese, aged mice. *Biology (Basel)*, **13**(12): 955.

Li W, Jiang L, Lu X, Liu X and Ling M (2021). Curcumin protects radiation-induced liver damage in rats through the NF-κB signaling pathway. *BMC Complement Med Ther*., **21**(1): 10.

Liao D, Shangguan D, Wu Y, Chen Y, Liu N, Tang J, Yao D and Shi Y (2023). Curcumin protects against doxorubicin induced oxidative stress by regulating the Keap1-Nrf2-ARE and autophagy signaling pathways. *Psychopharmacology (Berl)*., **240**(5): 1179-1190.

Lvova MN, Ponomarev DV, Tarasenko AA, Kovner A V, Minkova GA, Tsyganov MA, Li M, Lou Y, Evseenko VI, Dushkin AV, Sorokina IV, Tolstikova T G, Mordvinov VA and Avgustinovich DF (2023). Curcumin and its supramolecular complex with disodium glycyrrhizinate as potential drugs for the liver fluke infection caused by opisthorchis felineus. *Pathogens.*, **12**(6): 819.

Ma K, Shen Y, Hu J, Li J and Zhang X (2025). Curcumin as a therapeutic agent in liver cancer: A systematic review of preclinical models and mechanisms. *Eur J Med Res*.,**30**(1):640.

Meshanni JA, Lee JM, Vayas KN, Sun R, Jiang C, Guo GL, Gow AJ, Laskin JD and Laskin DL (2024). Suppression of lung oxidative stress, inflammation and fibrosis following nitrogen mustard exposure by the selective farnesoid X receptor agonist obeticholic acid. *J Pharmacol Exp Ther*., **388**(2): 586–595.

Pouliquen DL, Boissard A, Henry C, Coqueret O and Guette C (2022). Curcuminoids as modulators of EMT in invasive cancers: A review of molecular targets with the contribution of malignant mesothelioma studies. *Front Pharmacol..*,**13**:934534.

Ran Y, Su W, Gao F, Ding Z, Yang S, Ye L, Chen X, Tian G, Xi J and Liu Z (2021). Curcumin ameliorates white matter injury after ischemic stroke by inhibiting microglia/macrophage pyroptosis through NF-κB suppression and NLRP3 inflammasome inhibition. *Oxid Med Cell Longev*., **2021**:1552127.

Su J, Liu X, Zhao X, Ma H, Jiang Y, Wang X, Wang P, Zhao M and Hu (2025). Curcumin inhibits the growth of hepatocellular carcinoma *via* the MARCH1-mediated modulation of JAK2/STAT3 signaling. *Recent Pat Anticancer Drug Discov*., **20**(2): 145-157.

Tabanelli R, Brogi S and Calderone V (2021). Improving curcumin bioavailability: Current strategies and future perspectives. *Pharmaceutics*, **13**(10): 1715.

Tan X, Ma X, Dai Y, An J, Yu X, Li S, Liao Y, Pei T, Tang Y, Gui Y, Zhou S, Guo D, Deng Y Hu K and Wang D (2023). A large-scale transcriptional analysis reveals herb-derived ginsenoside F2 suppressing hepatocellular carcinoma via inhibiting STAT3. *Phytomedicine*, **120**: 155031.

Tian F, Chen T, Xu W, Fan Y, Feng X, Huang Q and Chen J (2023). Curcumin compensates GLP-1 deficiency via the microbiota-bile acids axis and modulation in functional crosstalk between TGR5 and FXR in ob/ob mice. *Mol Nutr Food Res*., **67**(22): e2300195.

Wang X, Tian Y, Lin H, Cao X and Zhang Z (2023). Curcumin induces apoptosis in human hepatocellular carcinoma cells by decreasing the expression of STAT3/VEGF/HIF-1α signaling. *Open Life Sci.*, **18**(1): 20220618.

Wang W, Li L, Li X, Chen J, Wang R, Yang Q, Qu Y, Wang C, Fu T and Meng Q (2025). FXR overexpression alleviates cholestasis via NLRC4 inflammasome suppression and bile acid homeostasis regulation. *Free Radic Biol Med*., **238**: 152–168.

Xie AJ, Mai CT, Zhu YZ, Liu XC and Xie Y (2021). Bile acids as regulatory molecules and potential targets in metabolic diseases. *Life Sci*., **287**: 120152.

Xu G, Gu Y, Yan N, Li Y, Sun L and Li B (2021). Curcumin functions as an anti-inflammatory and antioxidant agent on arsenic-induced hepatic and kidney injury by inhibiting MAPKs/NF-κB and activating Nrf2 pathways. *Environ Toxicol*., **36**(11): 2161-2173.

Zoi V, Galani V, Lianos GD, Voulgaris S, Kyritsis AP and Alexiou GA (2021). The role of curcumin in cancer treatment. *Biomedicines*., **9**(9): 1086.

Zhu F, Zheng S, Zhao M, Shi F, Zheng and Wang H (2023). The regulatory role of bile acid microbiota in the progression of liver cirrhosis. *Front Pharmacol*., **14**: 1214685.

Zhu J and He L (2024). The modulatory effects of curcumin on the gut microbiota: A potential strategy for disease treatment and health promotion. *Microorganisms*., **12**(4): 642.